

Ethylene oxides as hydrogen storage material with pockets in the electronic binding energy distribution

Sungjong Woo¹ and Young-Kyun Kwon^{1,2,*}¹*Department of Physics and Applied Physics and Nanomanufacturing Center of Excellence, University of Massachusetts, Lowell, Massachusetts 01854, USA*²*Department of Physics and Research Institute for Basic Sciences, Kyung Hee University, Seoul 130-701, Korea*

(Received 26 September 2008; revised manuscript received 29 December 2008; published 2 February 2009)

Using *ab initio* calculations, we have found that the oxygen atoms in oligomers of ethylene oxide have optimal binding with hydrogen molecules for hydrogen storage. Our theoretical model and molecular-dynamics simulations predict that adsorption-desorption process for such a candidate material occurs under unprecedented “ambient conditions,” $T \approx 300$ K and $P = 1-13$ atm, achieving gravimetric storage capacity of hydrogen up to 6.2 wt %. We have also uncovered the special binding mechanism between a hydrogen molecule and an oxygen-embedded material which is enhanced by electron donation and back-donation.

DOI: [10.1103/PhysRevB.79.075404](https://doi.org/10.1103/PhysRevB.79.075404)

PACS number(s): 61.46.-w, 68.43.Bc, 68.43.De, 84.60.Ve

I. INTRODUCTION

Hydrogen is a major research focus for future energy that would supersede the polluting fossil fuels which will be depleted in the near future. One of the most serious bottlenecks in this field is the storage of hydrogen. In order to store hydrogen more than 6% by weight set by U.S. Department of Energy (DOE) as the 2010 target, there have been several technologies proposed and tested including high-pressure tank,¹ liquid hydrogen, metal hydrides,² chemical hydrides,³ and physisorption on materials with large specific surfaces.⁴ None of them are, however, satisfactory up to date due to various obstacles encountered.⁵⁻⁷ The physisorption method has several advantages over the other methods, such as usage recyclability, adsorption kinetics, and so on, although its main disadvantage—the binding is too weak for molecular hydrogen to be stored near ambient condition as seen in graphitic carbon materials⁸⁻¹¹—should be overcome. In our previous research, materials with stronger physisorption binding than graphitic carbon materials were found such as boron nitrides¹² and boron oxides.^{13,14} The binding of which, however, was still not fully satisfactory.

In this paper, we report on certain molecules based on ethylene oxides ($-\text{OCH}_2\text{CH}_2-$) that have optimal binding energies for adsorption-desorption process under ambient conditions, $T \approx 300$ K and $P = 1-13$ atm, with gravimetric storage capacity of hydrogen up to 6.2 wt %, which should be readily observable in experiments. The stronger physical binding comes from the oxygen atom in the ethylene oxide. By analyzing the orbital mixing, we have found that such binding, which had also been observed in different contexts while had not been fully understood,¹⁵⁻¹⁷ is due to the electron donation and back-donation between the hydrogen molecule and the lone pairs of the oxygen atom.

In Sec. II, we describe our computational methods that have been used to investigate the system. In Sec. III, zero-temperature binding energies of hydrogen molecules on crown ether (CE) are presented. In Secs. IV and V, a thermodynamic model based on the calculated binding energies and the results of molecular-dynamics (MD) simulations are presented in order to study the adsorption-desorption process

at finite temperature. In Sec. VI, the binding mechanism between crown ether and a hydrogen molecule is explained. We conclude the paper in Sec. VII.

II. COMPUTATIONAL METHODS

To investigate the molecular hydrogen adsorption on ethylene oxides, we used the pseudopotential density-functional technique.¹⁸ The generalized gradient approximation (GGA) was used for the exchange-correlation of electrons,¹⁹ which is believed to be better than the local-density approximation (LDA) in describing gas adsorption.²⁰ Atomic orbitals with double- ζ polarization were used to expand single-particle wave functions²¹ with a cutoff energy of 100 Ry for the real-space mesh. We used 0.02 Ry for the confinement energy shift which defines the cutoff radii of the atomic orbitals. Relaxations of atomic structures were done using conjugate gradient method²² until the Hellmann-Feynman force on every atom becomes less than 1.56×10^{-3} Ry/ a_B with the Bohr radius a_B . All the calculations were done in a periodic cubic unit cell with a size of $20 \times 20 \times 20$ Å³.

III. BINDING ENERGIES

First we present our study of hydrogen adsorption on crown ether, a circular form of ethylene oxides. Depending on the number of ethylene oxides, there are different kinds of crown ether ($3n$ -crown- n , where $n \geq 4$ is the number of ethylene oxides or oxygen atoms), among which the lightest one, 12-crown-4, was investigated. To begin with, the structure of 12-crown-4 was relaxed finding that in the minimum-energy configuration oxygen atoms alternate their positions above and below the overall crown-ether plane [Fig. 1(a)]. Such an alternating oxygen configuration reduces the interaction energy between hydrogen atoms in the crown ether since otherwise the oxygen atoms are placed too close to each other.²³

We then calculated the total energy of a combined system of the relaxed crown ether and a hydrogen molecule as a function of the location of the hydrogen molecule around the crown ether. For each position, the calculations were done

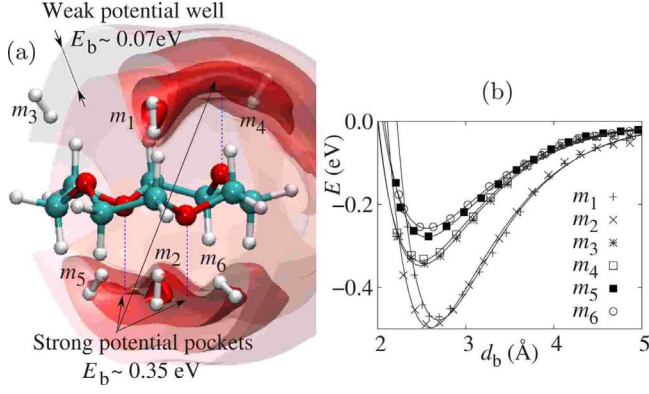


FIG. 1. (Color online) (a) 12-crown-4 with six hydrogen molecules m_1 – m_6 located at their energy minima. Dark gray (or red), gray (or green), and white balls represent oxygen, carbon, and hydrogen atoms, respectively. Four isosurfaces corresponding to energies of -0.05 , -0.11 , -0.25 , and -0.38 eV are drawn in order to show the potential pockets, where 0 eV is defined as the energy when the hydrogen molecule is far enough from the crown ether. Darker color represents lower energy. Gray (or blue) dashed lines are drawn to clarify which oxygen is related to which potential pocket. (b) Energy vs d_b curves for m_1 – m_6 in (a) where d_b is defined as the distance of each hydrogen molecule from the nearest oxygen atom.

for 13 different orientations of the hydrogen molecule and the minimum-energy orientation was chosen. Figure 1(a) shows the energy isosurfaces where darker gray (or red) color represents stronger binding energy. It is noted that there are four crescent-looking potential pockets for H_2 , each of which is generated around each oxygen atom. Two oxygen atoms above the crown-ether plane form two independent potential pockets that are spatially connected and so do the other two oxygen atoms below. The depth of these potential pockets is ~ 0.35 eV. The potential depth of the regions where two pockets overlap is even larger (~ 0.45 eV). One can also find a weaker potential well surrounding the crown ether, the depth of which is close to the molecular hydrogen binding energy for typical graphitic materials (~ 0.07 eV).

In order to see how many hydrogen molecules can be stored within the potential pockets, hydrogen molecules were added one after another to crown ether. Six different trajectories were chosen, two of which are on the vertical axis of the crown ether, whereas the other four are “diagonally” toward four oxygen atoms, respectively. Along each trajectory, a binding energy curve was obtained by calculating the total energies at varying binding distances d_b defined between H_2 and the closest oxygen atom [Fig. 1(b)]. At each fixed d_b , full relaxation of atomic positions was carried out. In Fig. 1(a), the six hydrogen molecules, indexed by m_1 – m_6 , are placed at their equilibrium positions with their most stable orientations. In Fig. 1(b), curves corresponding to m_1 and m_2 that have binding energy $E_b \sim 0.45$ eV are for the regions where two potential pockets overlap, whereas the other four curves ($E_b \sim 0.35$ eV) are for the four potential pockets. Two strongest binding sites corresponding to m_1 and m_2 , however, do not affect the overall behavior of the system since their sizes in the configuration space are much smaller than those of the

potential pockets around the oxygen atoms. Moreover, such strongest binding sites due to overlapping of two potential pockets are not “dynamically” stable as seen in our MD simulations, and thus such binding sites would not exist in a real system.²⁴ Figure 1(b) also shows that the hydrogen molecules attached to their equilibrium positions or pockets in the crown ether are energetically independent. Therefore one can say that four hydrogen molecules are bound to the four oxygen atoms in crown ether with $E_b \sim 0.35$ eV and about two additional hydrogen molecules can also be attached with smaller E_b due to the large sizes of binding pockets.

We have also checked the effect of zero-point vibrational energy shift of a bound hydrogen molecule using frozen phonon method. Differently from work of Lee *et al.*,²⁵ the calculated frequency shift was very minimal—only 0.07% of the vibrational frequency of a free hydrogen molecule—which, therefore, can be ignored. This is attributed by the fact that in the case of Lee *et al.* each hydrogen molecule is bound to the metal atom *transversely* with the H_2 bond length significantly elongated, while in our case it is bound to the oxygen atom *axially* with its bond length barely affected.

IV. THERMODYNAMIC MODEL

To understand adsorption-desorption behaviors at various temperatures and pressures, we have developed a theoretical model based on thermodynamics with the information obtained from the above binding energy calculations. It is assumed that crown ether has six independent potential wells, each of which can bear one hydrogen molecule with binding energy ϵ_i , where $i = 1, \dots, 6$. Such a system can be described by a mixture of eight chemical species: CE, H_2 , and nH_2 -CE representing bound states of crown ether with n hydrogen molecules ($n = 1, \dots, 6$). The reaction equations between different nH_2 -CE combinations can be written as $H_2 + (n-1)H_2\text{-CE} \rightleftharpoons nH_2\text{-CE}$. Equating the chemical potentials on both sides yields

$$\begin{aligned} (N_{H_2}^{\text{tot}} - N_{H_2}) \sum_{n=0}^6 K^n N_{H_2}^n \exp\left(-\frac{F_{nH_2\text{-CE}}}{k_B T}\right) \\ = \sum_{n=1}^6 n K^n N_{H_2}^n \exp\left(-\frac{F_{nH_2\text{-CE}}}{k_B T}\right) \end{aligned} \quad (1)$$

for a system consisting of crown ether and $N_{H_2}^{\text{tot}}$ hydrogen molecules in a fixed volume V at temperature T , where N_{H_2} is the number of free hydrogen molecules, $K \equiv (n_{q,H_2} V)^{-1}$, $n_{q,H_2} = (M_{H_2} k_B T / 2\pi\hbar^2)^{3/2}$ is the quantum concentration of H_2 , M_{H_2} is the mass of H_2 , and $F_{nH_2\text{-CE}} \equiv -k_B T \ln[n! \sum_{i_1=n}^6 \dots \sum_{i_{n-1}=1}^{(i_{n-1}-1)} e^{-(\epsilon_{i_1} + \dots + \epsilon_{i_n})/k_B T}]$ is the internal free energy (see the Appendix for detailed derivation).

By solving Eq. (1) numerically in terms of N_{H_2} , the number of adsorbed hydrogen molecules $N_{H_2}^{\text{ads}} = N_{H_2}^{\text{tot}} - N_{H_2}$ can be determined and so can the pressure P using the van der Waals (vdW) equation of state. In Fig. 2, the shaded area shows the transition region in the P - T space where $1 < N_{H_2}^{\text{ads}} < 5$. For the calculation, the binding energies are given by

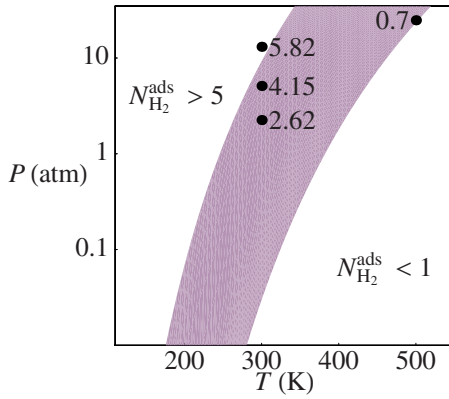


FIG. 2. (Color online) Results of the theoretical thermodynamics model: the shaded area represents the transition region where the number of bound hydrogen molecules is between 1 and 5. Its left side is fully adsorbed region while the right side is fully desorbed region. The number of adsorbed hydrogen molecules from MD simulations is given in the figure with corresponding dots.

the three-dimensional (3D) potential calculations; $\epsilon_{1-4} = 0.35$ eV and $\epsilon_{5,6} = 0.2$ eV. It is noted that a room-temperature adsorption-desorption process is possible under moderate pressure.

V. MOLECULAR-DYNAMICS SIMULATION

We then performed finite-temperature MD simulations regulated by Nosé thermostat^{26,27} in order to check our thermodynamic model. We used a cubic unit cell of volume $8.0 \times 10^3 \text{ \AA}^3$, in which crown ether and $N_{\text{H}_2}^{\text{tot}}$ hydrogen molecules were randomly distributed at $T=300$ and 500 K. During each simulation at every time step of 5.0×10^{-16} s, the distance of each H_2 from the center of mass of crown ether, r , was recorded in order to obtain stochastic probability density. Figure 3 shows the probability densities of H_2 as a function of r . For each histogram, a significant peak is identified within $2 \leq r \leq 7 \text{ \AA}$ which represents bound hydrogen molecules. A distribution for free hydrogen molecules is also found in the region where $r \geq 7 \text{ \AA}$ which is proportional to r^2 . A Gaussian distribution function with an asymmetric Lorentzian tail, $f(r)$, was used to fit the bound region whereas a quadratic function with a smooth lower cutoff, $g(r)$, was used to describe the r^2 behavior of free hydrogen molecules. Once the fitting is done, $N_{\text{H}_2}^{\text{ads}}$ can be obtained by integrating $f(r)$ while P can be extracted from the coefficient of $g(r)$ using the vdW equation of state. Our MD simulations were carried out up to 300 000 time steps (~ 150 ps) which is enough to estimate the statistics; at least 10 times of H_2 adsorption-desorption events were monitored during each MD simulation.

From Fig. 3(a) obtained for $N_{\text{H}_2}^{\text{tot}}=3$ and $T=300$ K, it is estimated that $N_{\text{H}_2}^{\text{ads}}=2.62$ and $P=2.25$ atm. By increasing $N_{\text{H}_2}^{\text{tot}}$ to 5 and 8 at the same temperature [Figs. 3(b) and 3(c)], $N_{\text{H}_2}^{\text{ads}}=4.15$ and 5.82 at $P=5.11$ and 13.1 atm, respectively. As a promising result, $N_{\text{H}_2}^{\text{ads}}=5.82$ corresponds to 6.20 wt %. Increasing the temperature to $T=500$ K with $N_{\text{H}_2}^{\text{tot}}=3$ reveals

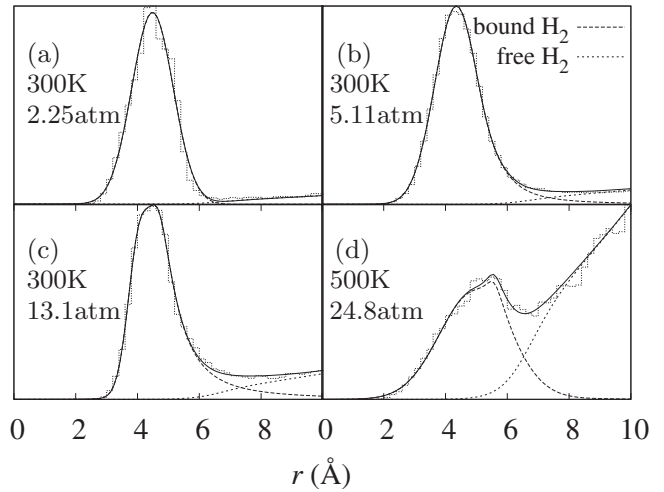


FIG. 3. Probability density plots of hydrogen molecules as a function of the distance from the center of the crown ether. The peaks under 7 \AA represent the bound hydrogen molecules and the density above 7 \AA represents free ones. By comparing (a)–(c) and (d), it is obvious that raising temperature pushes hydrogen molecules to the continuum level from the bound state. More details including the fitting are in the text.

very efficient desorption behavior; the probability density outside the bound region ($d \geq 7 \text{ \AA}$) increases significantly [Fig. 3(d)], so that $N_{\text{H}_2}^{\text{ads}}=0.7$ even at a very high pressure of $P=24.8$ atm. Our MD simulation results are in a good agreement with our theoretical model—the simulated $N_{\text{H}_2}^{\text{ads}}$ for each T and P is written in Fig. 2.

VI. OXYGEN LONE-PAIR BINDING MECHANISM

Next, we have investigated why the binding is stronger than that of a typical physisorption. For this purpose we used polyethylene glycol (PEG), a polymer form of ethylene oxides [Fig. 4(a)], since we already confirmed that the strong interaction comes from the oxygen atoms in crown ether *not from the ring-shaped structure*. Two paths I and II were chosen for H_2 to approach toward PEG. Path I passes through the crescent-shaped potential pocket around an oxygen atom. Path II approaches from the opposite side—along this path the effect of oxygen atom located at the opposite side of PEG is screened by other atoms. The binding energy curves [Fig. 4(b)] show stronger binding ($E_b \geq 0.3$ eV) for path I and weaker binding ($E_b \leq 0.1$ eV) for path II. We found that the induced electric dipole moment of H_2 , P_{H_2} , increases as d_b decreases for both paths, while solely for path I a charge transfer from the crown ether toward H_2 also increases as d_b decreases [Figs. 4(c) and 4(d)]. It is also noted that the charge transfer occurs mainly from the oxygen atom. This implies that the charge transfer between the crown ether and H_2 for path I forms an electron donor-acceptor complex while both paths involve induced dipole interaction.

In order to see this point more clearly, electronic orbitals of the system were studied. It is known that, if there is a level mixing (orbital hybridization) between orbitals above and below the Fermi level, the total energy of the ground-state

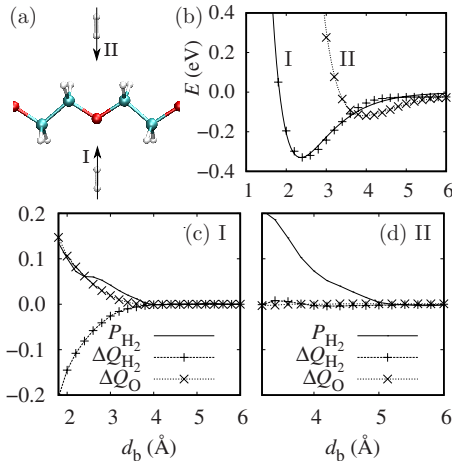


FIG. 4. (Color online) (a) PEG within a periodic unit cell and two hydrogen molecules at their respective energy minima along two paths I and II. (b) Similar curves as in Fig. 1(b) for the case of PEG. As in crown ether, the energy minimum for hydrogen binding along path I is found at $d_b \sim 2.4$ Å with $E_b \approx 0.3$ eV, while for the other path along which the oxygen is screened by other atoms the potential depth is $E_b \leq 0.1$ eV. P_{H_2} curves in (c) and (d) show the induced dipole moment on each H_2 in the dimension of $e \times \text{Å}$, where $-e$ is the charge of an electron. ΔQ_i in (c) and (d) represent the change in charge given in e on the element i as a function of d_b . To get the electric charge on each atom, Mulliken population is used.

electronic configuration will be lowered due to the level repulsion. Here, we denote the nonhybridized molecular orbitals as ϕ_i and the hybridized ones between H_2 and PEG as ψ_i , where i is the index of each energy level. Figure 5(a) shows three selected nonhybridized orbitals near the Fermi level for the case of path I. The first two orbitals ϕ_1 and ϕ_2 are those below the Fermi level while ϕ_3 represents the one above. Since H_2 is far enough from the PEG, H_2 $s\sigma$ orbital (ϕ_1) and $s\sigma^*$ orbital (ϕ_3) are fully decoupled from the PEG orbitals. Figure 5(b) depicts hybridized orbitals ψ_1 and ψ_2 between ϕ_1 and ϕ_2 when H_2 is located at the energy minimum of the oxygen potential pocket; ψ_1 is the bonding (lower energy) and ψ_2 is the antibonding (higher energy). Note that only the oxygen p_z orbital that has the lone pairs is significantly involved. This hybridization, however, cannot directly lower the total energy since both ϕ_1 and ϕ_2 are under the Fermi level. For more quantitative analysis, we have projected ψ_i onto ϕ_i such that $\psi_i = \sum_j M_{ij} \phi_j$. Black bar charts (upper part) in Figs. 5(c) and 5(d) visualize the population vectors ($M_{i1}^2, M_{i2}^2, M_{i3}^2$) for ψ_1 and ψ_2 , respectively. A vertical dashed line is drawn in each plot to show the Fermi level. From the bar charts one can note that ψ_2 involves hybridization not only with ϕ_1 but also with ϕ_3 ; we have observed that, among the ψ_i 's below the Fermi level, this level mixing is the largest contribution from any ϕ_i above the Fermi level. In ψ_2 , the H_2 $s\sigma$ orbital is slightly shifted further away from PEG. This could be simply due to the antibonding between ϕ_1 and oxygen p_z orbital in ϕ_2 but it could also be interpreted as a mixture of ϕ_1 slightly with ϕ_3 that makes bonding with the oxygen p_z orbital. In other words, the hybridization of ϕ_2 with ϕ_1 enhances the transition amplitude from such a first-

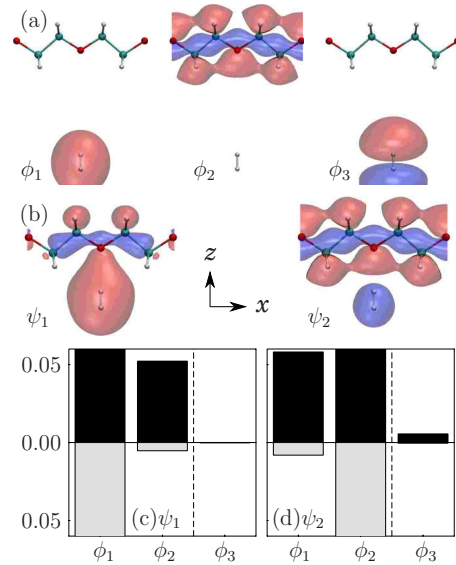


FIG. 5. (Color online) (a) Three selected nonhybridized orbitals: ϕ_1 and ϕ_2 are below the Fermi level while ϕ_3 is above the Fermi level. (b) Hybridized orbitals for hydrogen binding along path I at $d_b = 2.4$ Å: ψ_1 is a bonding while ψ_2 is an antibonding of ϕ_1 and ϕ_2 . The black bar charts in (c) and (d) show the amount of hybridizations in ψ_1 and ψ_2 . The gray bar charts show the counterpart along path II.

hybridized state to ϕ_3 yielding a second-hybridized ψ_2 orbital. It can also be interpreted that the electrons are donated from the H_2 $s\sigma$ orbital to a higher-energy oxygen p_z orbital in the PEG, elevating the energy of a part of the electrons in the H_2 $s\sigma$ orbital, so that they can be back-donated to H_2 $s\sigma^*$ orbital. On the other hand, gray bar charts show the corresponding plots for the case of path II at its energy minimum. In Fig. 5(d), the gray bar chart (lower part), differently from the black bar chart, has no contribution from ϕ_3 . This is due to the lack of significant mixing between ϕ_1 and ϕ_2 . O- H_2 binding reveals another nonclassical mechanism that is different from the known B- H_2 binding²⁸ in that one involves the doubly occupied lone pairs of O while the other must involve empty p_z orbitals of B.

VII. CONCLUSION

In conclusion, oligomers of ethylene oxide have optimal binding energy for molecular hydrogen storage with high gravimetric capacity up to ~ 6.2 wt % for 12-crown-4 as well as good desorption process under ambient conditions of temperature and pressure. We found that the special mixing between the hydrogen molecular orbitals and the lone pairs of the oxygen atom in ethylene oxide occurs through electron donation and back-donation that give the special binding strength. It is, however, noted that our promising result is based on single crown ether and would not be realistic in liquid crown ether due to the ether-ether intermolecular interaction. Our eventual goal is to build and investigate crown-ether-based porous materials in a form of covalent organic framework.²⁹ Such a framework would keep the optimum hydrogen binding energy while minimizing ether-

ether interactions as well as maximizing the surface area for H_2 storage. Our finding should encourage experimentalists to test the material and open up a ambient-condition high-capacity hydrogen storage technique.

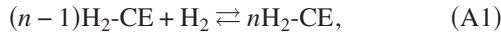
ACKNOWLEDGMENTS

The authors acknowledge S.-H. Jhi, Y.-J. Jung, D. Schmidt, J. Therrien, and M. Yoon for useful discussions. This work was supported partially by Nanomanufacturing Center of Excellence and used the computational resources at the National Energy Research Scientific Computing Center supported by the Office of Science of the U.S. Department of Energy under Contract No. DE-AC02-05CH11231.

APPENDIX: HYDROGEN ADSORPTION-DESORPTION MODEL ON CROWN ETHER

We are going to describe a simple model to find out the average number of adsorbed hydrogen molecules on crown ether when the total number of hydrogen molecules, $N_{H_2}^{\text{tot}}$, in a fixed volume V is given under certain temperature T . It is assumed that crown ether has six independent potential wells, each of which can bear only one hydrogen molecule—the binding energy of additional hydrogen molecules to a potential pocket which is already occupied is substantially smaller than the first one. Such a system can be described by a mixture of eight chemical species: CE, H_2 , and nH_2 -CE, where CE represents crown ether and nH_2 -CE represents a bound state of n hydrogen molecules on crown ether with $n=1, \dots, 6$.

The reaction equations for different combinations of crown ether and hydrogen molecules can be written as



where $n=1, \dots, 6$. In equilibrium, the chemical potentials should be the same on both sides of Eq. (A1),

$$\mu_{(n-1)H_2\text{-CE}} + \mu_{H_2} = \mu_{nH_2\text{-CE}}, \quad n=1, \dots, 6. \quad (\text{A2})$$

By approximating the system as classical ideal gas, the chemical potential of species i is

$$\mu_i = k_B T \ln n_i - k_B T \ln n_{q,i} + F_i, \quad (\text{A3})$$

where k_B is the Boltzmann constant, $n_i = N_i/V$ is the gas density, $n_{q,i} = (M_i k_B T / 2\pi\hbar^2)^{3/2}$ is the quantum concentration, and F_i is the internal free energy due to the binding.³⁰ Considering hydrogen atoms as distinguishable particles³¹ and $F_{CE} = F_{H_2} = 0$, the free energy of nH_2 -CE is

$$F_{nH_2\text{-CE}} = -k_B T \ln \left\{ n! \sum_{j_1=n}^6 \sum_{j_2=n-1}^{j_1-1} \cdots \sum_{j_n=1}^{(j_{n-1})-1} e^{-(E_{j_1} + \cdots + E_{j_n})/k_B T} \right\}, \quad (\text{A4})$$

where E_j is the binding energy of the j th potential well. Substituting Eqs. (A3) and (A4) into Eq. (A2) yields

$$N_{nH_2\text{-CE}} = K_n(T, V) N_{(n-1)H_2\text{-CE}} N_{H_2} \times \exp\left(\frac{F_{nH_2\text{-CE}} - F_{(n-1)H_2\text{-CE}}}{k_B T}\right), \quad (\text{A5})$$

where

$$K_n(T, V) = \frac{1}{V n_{q,H_2}} \left(\frac{M_{(n-1)H_2\text{-CE}}}{M_{nH_2\text{-CE}}}\right)^{-3/2}. \quad (\text{A6})$$

Here, $K_n(T, V)$ can be approximated to be independent of n since $M_{CE} \gg M_{H_2}$,

$$K_n(T, V) \approx (V n_{q,H_2})^{-1} \equiv K(T, V), \quad (\text{A7})$$

so that Eq. (A5) becomes

$$N_{nH_2\text{-CE}} = K(T, V) N_{(n-1)H_2\text{-CE}} N_{H_2} \exp\left(\frac{F_{nH_2\text{-CE}} - F_{(n-1)H_2\text{-CE}}}{k_B T}\right). \quad (\text{A8})$$

The assumed constraint number of the total hydrogen molecules and the crown ether gives two constraint equations:

$$N_{H_2}^{\text{tot}} = N_{H_2} + \sum_{n=1}^6 n N_{nH_2\text{-CE}}, \quad (\text{A9})$$

$$N_{CE}^{\text{tot}} = \sum_{n=0}^6 N_{nH_2\text{-CE}} \equiv 1. \quad (\text{A10})$$

From Eq. (A8), one can get

$$N_{nH_2\text{-CE}} = K^n N_{CE} N_{H_2}^n \exp\left(-\frac{F_{nH_2\text{-CE}}}{k_B T}\right). \quad (\text{A11})$$

Substituting Eq. (A11) into Eqs. (A9) and (A10) gives

$$N_{H_2}^{\text{tot}} - N_{H_2} = N_{CE} \sum_{n=1}^6 n K^n N_{H_2}^n \exp\left(-\frac{F_{nH_2\text{-CE}}}{k_B T}\right), \quad (\text{A12})$$

$$1 \equiv N_{CE}^{\text{tot}} = N_{CE} \sum_{n=0}^6 K^n N_{H_2}^n \exp\left(-\frac{F_{nH_2\text{-CE}}}{k_B T}\right). \quad (\text{A13})$$

By eliminating N_{CE} from Eqs. (A12) and (A13), one can get a seventh-order polynomial equation of N_{H_2} ,

$$(N_{H_2}^{\text{tot}} - N_{H_2}) \sum_{n=0}^6 K^n N_{H_2}^n \exp\left(-\frac{F_{nH_2\text{-CE}}}{k_B T}\right) = \sum_{n=1}^6 n K^n N_{H_2}^n \exp\left(-\frac{F_{nH_2\text{-CE}}}{k_B T}\right). \quad (\text{A14})$$

Solving Eq. (A14) gives the average number of adsorbed hydrogen molecules, $N_{H_2}^{\text{ads}} \equiv N_{H_2}^{\text{tot}} - N_{H_2}$, as a function of $N_{H_2}^{\text{tot}}$ and T in a fixed volume V . Since the pressure of the system, P , can also be calculated using the van der Waals equation, N_{H_2} can be represented as a function of P and T indirectly.

*Corresponding author. ykkwon@khu.ac.kr

- ¹M. Cumalioglu, Y. Ma, A. Ertas, and T. Maxwell, *J. Pressure Vessel Technol.* **129**, 216 (2007).
- ²J. Chen, N. Kuriyama, H. T. Takeshita, H. Tanaka, T. Sakai, and M. Haruta, *Electrochem. Solid-State Lett.* **3**, 249 (2000).
- ³J. Huot, G. Liang, and R. Schulz, *J. Alloys Compd.* **353**, L12 (2003).
- ⁴N. L. Rosi, J. Eckert, M. Eddaoudi, D. T. Vodak, J. Kim, M. O’Keeffe, and O. M. Yaghi, *Science* **300**, 1127 (2003).
- ⁵M. S. Dresselhaus *et al.*, *Report of the Basic Energy Sciences Workshop on Hydrogen Production, Storage, and Use, May 13–15, 2003* (2nd printing, 2004), and references therein. Available at <http://www.sc.doe.gov/bes/hydrogen.pdf>.
- ⁶R. Coontz and B. Hanson, *Science* **305**, 957 (2004).
- ⁷G. W. Crabtree, M. S. Dresselhaus, and M. V. Buchanan, *Phys. Today* **57** (12), 39 (2004).
- ⁸A. C. Dillon, K. M. Jones, T. A. Bekkedahl, C. H. Kiang, D. S. Bethune, and M. J. Heben, *Nature (London)* **386**, 377 (1997).
- ⁹C. Liu, Y. Y. Fan, M. Liu, H. T. Cong, H. M. Cheng, and M. S. Dresselhaus, *Science* **286**, 1127 (1999).
- ¹⁰M. A. de la Casa-Lillo, F. Lamari-Darkrim, D. Cazorla-Amoros, and A. Linares-Solano, *J. Phys. Chem. B* **106**, 10930 (2002).
- ¹¹N. Texier-Mandoki, J. Dentzer, T. Piquero, S. Saadallah, P. David, and C. Vix-Guterl, *Carbon* **42**, 2744 (2004).
- ¹²S.-H. Jhi and Y.-K. Kwon, *Phys. Rev. B* **69**, 245407 (2004).
- ¹³S.-H. Jhi and Y.-K. Kwon, *Phys. Rev. B* **71**, 035408 (2005).
- ¹⁴S.-H. Jhi, Y.-K. Kwon, K. Bradley, and J. P. C. Gabriel, *Solid State Commun.* **129**, 769 (2004).
- ¹⁵R. E. Pritchard, M. J. Ashwin, J. H. Tucker, and R. C. Newman, *Phys. Rev. B* **57**, R15048 (1998).
- ¹⁶V. P. Markevich, M. Suezawa, and L. I. Murin, *Mater. Sci. Eng., B* **58**, 26 (1999).
- ¹⁷S.-H. Jhi, *Phys. Rev. B* **74**, 155424 (2006).
- ¹⁸M. L. Cohen, *Phys. Scr.* **T1**, 5 (1982).
- ¹⁹J. P. Perdew, K. Burke, and M. Ernzerhof, *Phys. Rev. Lett.* **77**, 3865 (1996).
- ²⁰There is a question whether GGA (or LDA) could describe correctly the van der Waals interaction due to its long-range nature. Recently several attempts have been made to incorporate the van der Waals interaction into the density-functional theory but none of them have yet reached the level of a consistent and reliable methodology; for example, see J. P. Perdew, K. Burke, and M. Ernzerhof, *Phys. Rev. Lett.* **77**, 3865 (1996); E. Hult, Y. Andersson, B. I. Lundqvist, and D. C. Langreth, *ibid.* **77**, 2029 (1996); W. Kohn, Y. Meir, and D. E. Makarov, *ibid.* **80**, 4153 (1998); H. Rydberg, M. Dion, N. Jacobson, E. Schroder, P. Hyldgaard, S. I. Simak, D. C. Langreth, and B. I. Lundqvist, *ibid.* **91**, 126402 (2003), and references therein.
- ²¹D. Sanchez-Portal, P. Ordejon, E. Artacho, and J. M. Soler, *Int. J. Quantum Chem.* **65**, 453 (1997).
- ²²M. R. Hestenes and E. Stiefel, *J. Res. Natl. Bur. Stand.* **49**, 409 (1952).
- ²³S.-H. Jhi, *Microporous Mesoporous Mater.* **89**, 138 (2006), in which more symmetric crown-ether structures were used. We have checked the energies of both structures showing that our structure has lower energy by 1.45 eV even though both represent local energy minima.
- ²⁴The position of each potential pocket is tied to the position of corresponding oxygen atom. At finite temperature, the position of each oxygen atom fluctuates, so that the overlapping of two potential pockets will not be spatially stable.
- ²⁵H. Lee, W. I. Choi, and J. Ihm, *Phys. Rev. Lett.* **97**, 056104 (2006).
- ²⁶S. Nosé, *Mol. Phys.* **52**, 255 (1984).
- ²⁷W. G. Hoover, *Phys. Rev. A* **31**, 1695 (1985).
- ²⁸Y.-H. Kim, Y. Zhao, A. Williamson, M. J. Heben, and S. B. Zhang, *Phys. Rev. Lett.* **96**, 016102 (2006).
- ²⁹H. M. El-Kaderi, J. R. Hunt, J. L. Mendoza-Cortés, A. P. Côté, R. E. Taylor, M. O’Keeffe, and O. M. Yaghi, *Science* **316**, 268 (2007).
- ³⁰C. Kittel and H. Kroemer, *Thermal Physics*, 2nd ed. (Freeman, San Francisco, 1980), pp. 266–271.
- ³¹Due to the richness of the rovibrational modes, molecular hydrogens can be considered as nonidentical particles.